\*\*Volume Title\*\*
ASP Conference Series, Vol. \*\*Volume Number\*\*
\*\*Author\*\*
© \*\*Copyright Year\*\* Astronomical Society of the Pacific

### Aspects of Multi-Dimensional Modelling of Substellar Atmospheres

Ch. Helling<sup>1</sup>, E. Pedretti<sup>1</sup>, S. Berdyugina<sup>2</sup>, A.A. Vidotto<sup>1</sup>, B. Beeck<sup>3,4</sup>, E. Baron<sup>5,6</sup>, A.P. Showman<sup>7</sup>, E. Agol<sup>8</sup>, D. Homeier<sup>4</sup>

**Abstract.** Theoretical arguments and observations suggest that the atmospheres of Brown Dwarfs and planets are very dynamic on chemical and on physical time scales. The modelling of such substellar atmospheres has, hence, been much more demanding than initially anticipated. This Splinter<sup>1</sup> has combined new developments in atmosphere modelling, with novel observational techniques, and new challenges arising from planetary and space weather observations.

#### 1. Introduction

A rich molecular gas-phase chemistry coupled with cloud formation processes determines the atmosphere spectra of very low-mass, cool objects. Interferometry (E. Pedretti, Sect. 2) and polarimetry (S. Berdyugina, Sect. 3) can potentially provide more insight. However, present day interferometers are not capable of surface imaging Brown Dwarfs and planets due to financial constraints. Polarimetry, as a novel planet detection method, benefits from Rayleigh scattering on high-altitude sub- $\mu$ m cloud particles. Such clouds were predicted to form by non-equilibrium processes several years ago

<sup>&</sup>lt;sup>1</sup> SUPA, School of Physics & Astronomy, University St Andrews, St Andrews, North Haugh, KY16 9SS, UK

<sup>&</sup>lt;sup>2</sup> Kiepenheuer Institut für Sonnenphysik, Schöneckstr. 6, D-79104 Freiburg, Germany

<sup>&</sup>lt;sup>3</sup> Max Planck Institute for Solar-System Research, Max-Planck-Straße 2, 37191 Katlenburg-Lindau, Germany

<sup>&</sup>lt;sup>4</sup> Georg August University, Institute for Astrophysics, Friedrich-Hund-Platz 1, 37077 Göttingen, Germany

<sup>&</sup>lt;sup>5</sup>Homer L. Dodge Department of Physics and Astronomy, University of Oklahoma, 440 W Brooks, Rm 100, Norman, OK 73019 USA

<sup>&</sup>lt;sup>6</sup>Computational Research Division, Lawrence Berkeley National Laboratory, MS 50F-1650, 1 Cyclotron Rd, Berkeley, CA 94720 USA

<sup>&</sup>lt;sup>7</sup> Department of Planetary Sciences, University of Arizona, Tucson, AZ, USA

<sup>&</sup>lt;sup>8</sup>Dept. of Astronomy, Box 351580, University of Washington, Seattle, WA 98195

<sup>&</sup>lt;sup>1</sup>http://star-www.st-and.ac.uk/~ch80/CS16/MultiDSplinter\_CS16.html

(Woitke & Helling 2004). Wavelength dependent transit timing may reveal the interaction of the planetary exosphere with the stellar corona, and hence, limits may be set on planetary magnetic field strengths (A.A. Vidotto, Sect. 4). Radiative MHD simulations suggest that magnetic field driven convection significantly changes in fully convective objects compared to the Sun: M-dwarfs are suggested to exhibit darker magnetic structures (B. Beeck, Sect. 5). Studies of multi-dimensional radiative transfer emphasize that full solutions of physical problems are needed to access limits approximations (E. Baron, Sect. 6). The superrotation observed in planetary atmospheres is suggested to result from standing Rossby waves generated by the thermal forcing of the day-night temperature difference (A.P. Showman, Sect. 7). A search for transit-time variations at 8  $\mu$ m reveals a difference between the transit and the secondary eclipse timing after subtracting stellar variability, and hence, confirms the superrotation on HD 189733b (E. Agol, Sect. 8). Results of multi-dimensional simulations are starting to be used as input for 1D model atmospheres for synthetic spectra production (D. Homeier, Sect. 9).

#### 2. Combined interferometry for substellar variability (Ettore Pedretti)

Optical and infrared long-baseline interferometry allows high-resolution imaging that is out of reach for the current large telescope facilities and for the planned 30m class telescopes. Examples of typical and future targets for long-baseline interferometry are stellar surfaces, planet-forming discs, active galactic nuclei and extrasolar planets. The main interferometric facilities in the northern hemisphere are the center for high angular resolution astronomy (CHARA) array and the Keck interferometer. CHARA is a visible and infrared interferometer composed of 6 one-metre telescopes on a 330m maximum baseline (see Pedtretti et al. 2009). The Keck interferometer is composed of two 10m telescopes on a 85m baseline and works mainly in the infrared. The main facility in the southern hemisphere is the very large telescope interferometer (VLTI), composed of four 8m telescopes and four 2m telescopes on a 200m maximum baseline. The Sidney university stellar interferometer (SUSI) in Australia has the longest available baseline in the world (640m) but so far has only used up to 80m baselines. Previous generation interferometers provided unique science by measuring the diameters of stars with two telescopes or by providing simple model dependent imaging combining up to 3 telescopes (Berger et al. 2001, Monnier et al. 2003, Pedretti et al. 2009) Modelindependent imaging of complex objects was achieved quite recently at the CHARA array, that obtained the first image of a main-sequence star, Altair (Monnier et al. 2007). CHARA also imaged the most distant eclipsing system, the star  $\beta$  Lirae and witnessed the spectacular eclipse from the  $\epsilon$  Aur system (Kloppenborg et al. 2010; Fig. 1). The VLTI imaged the young stellar object IRAS 13481-6124 (Kraus et al. 2010).

An interesting question is whether interferometry could resolve brown dwarfs and provide the same sort of high–resolution pictures offered to its larger stellar cousins.  $\epsilon$  Indi B is the nearest brown dwarf (Scholz et al 2003). The distance is 3.6 pc, corresponding to an angular diameter of 0.3 milliarcseconds, and a magnitude at H band Mh = 11.3.  $\epsilon$  Indi B is in the southern hemisphere, therefore it is only accessible by the VLTI and SUSI. The VLTI does not have long enough baselines, its maximum baseline being 200m. SUSI with its 640m baselines would achieve in the infrared, at H band a resolution of 0.5 milliarcseconds, therefore it could measure the diameter and effective temperature of  $\epsilon$  Indi B if its bolometric flux was known. However SUSI has never used baselines longer than 80m and it is not sensitive enough to reach Mh = 11.3,

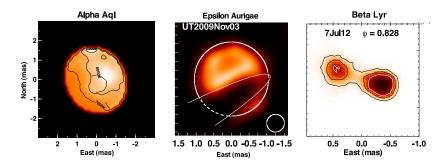


Figure 1. CHARA results. From left: Alpha Aql, first image of a main sequence star other than the Sun; the dust disc orbiting an unseen companion and eclipsing the star  $\epsilon$  Aurigae;  $\beta$  Lyr, the closest interacting binary star ever imaged.

since it uses small 10cm siderostats. Resolved imaging of brown-dwarfs is out of reach for the present interferometric facilities. Brown-dwarfs are at least as challenging to image as Jupiter-size planets. A facility the size of the Atacama large millimetre array (ALMA) at infrared wavelengths would possibly achieve imaging of brown-dwarfs and Jupiter-size planets but it is unlikely that such facility will be financed in the short term. The remaining question is what could existing interferometers do in term of science, other than resolved imaging of the atmosphere of a brown-dwarf. The recent detection of brown dwarfs in binary systems within 5 AU from the main star from Corot (see CoRoT-3b, CoRot-6b and Super-WASP soon) opens up interesting possibilities. Many rejected planets in radial-velocity surveys may be brown dwarfs therefore there may be a large number available targets. Interferometry could potentially characterise brown dwarfs in binary and multiple systems very close to a brighter, more massive companion star through precision closure-phase measurement (Zhao 2009). Closure-phase nulling (Chelli et al 2009) a special case of precision closure—phase, where measurement are performed around nulls of visibility function and produce large change of closure-phase is potentially more sensitive. Interferometry could yield spectral and flux information about the brown dwarf and derive the mass of the brown-dwarf by measuring the inclination of the orbit in combination with radial velocity measurements.

#### 3. Polarized Light in stars and planets (Svetlana Berdyugina)

Polarimetry is a powerful technique for revealing hidden structures in astrophysical objects, far beyond spatial resolution provided by direct imaging at any telescope. Polarization is a fundamental property of the light. It is its incredible sensitivity to asymmetries that empowers polarimetry and allows us to look inside unresolved structures. For instance, light can become polarized when it is scattered, or passes through magnetized matter, or is absorbed in an environment illuminated by anisotropic radiation.

Using molecular spectropolarimetry of cool stars enables us to obtain the first 3D view of starspots with the strongest field and the coldest plasma on the stellar surface. Such a phenomenon is common among stars possessing convective envelopes, where magnetic fields are believed to be generated (Berdyugina 2005). However, until recently magnetic fields have never been measured directly inside starspots. By selecting molecular lines which preferably form in cool starspots and at different heights in their atmosphere, such as TiO, CaH, and FeH, starspots and their internal structure are re-

solved (Berdyugina 2011). A new diagnostic technique of embedded stars and inner parts of protoplanetary disks based on radiative pumping of absorbers has been pioneered by (Kuhn et al. 2007). In the presence of anisotropic incident radiation, e.g. clumps of protoplanetary material illuminated by a star, the lower state magnetic sublevels of atoms or molecules in the intervening gas become unequally populated (even in the absence of magnetic fields). Such an 'optically pumped' gas will result in polarized line absorption along the line of sight. This provides novel insights into the structure and evolution of the innermost parts of circumstellar disks which are inaccessible to any other technique (Kuhn et al. 2011).

Detecting planetary atmospheres in polarized light provides a direct probe of exoplanets outside transits. The light scattered in the planetary atmosphere is linearly polarized and, when the planet revolves around the parent star, the polarization varies. Thus, the observed polarization variability exhibits the orbital period of the planet and reveals the inclination, eccentricity, and orientation of the orbit as well as the nature of scattering particles in the planetary atmosphere. HD189733b is a very hot Jupiter and the first exoplanet detected in polarized light (Berdyugina et al 2008). The observed polarization (Fig. 2) is caused by Rayleigh scattering, possibly on 20 nm MgSiO<sub>3</sub> dust condensates (Berdyugina 2011).

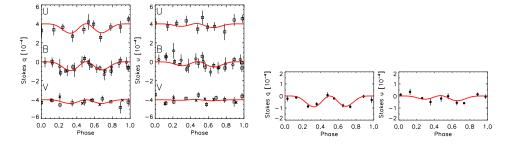


Figure 2. Polarimetric data (normalized Stokes q and u) for HD189733b in UBV bands. Left: squares – Berdyugina et al. (2011), open circles – binned B-band data from Berdyugina et al. (2008), crosses – broad-band filter data by Wiktorowicz (2009) centered at the V-band. The U and V data are shifted in vertical by  $\pm 4\cdot 10^{-4}$  for clarity. Right: All the U and B data from the years 2006-2008 binned together. The mean error of the binned data is  $1.7\cdot 10^{-5}$ . Curves are the best-fit solutions for a model atmosphere with Rayleigh scattering on dust particles.

#### 4. Stellar influence on planet atmosphere is shocking (Aline A. Vidotto)

WASP-12b is a transiting giant planet that was first identified in an optical photometric transit survey (Hebb et al. 2009). More recently, transit observations were also done in the near-UV (Fossati et al 2010a), revealing that while the time of the egress of the transit occurs almost simultaneously for both the optical and the near-UV observations, the ingress is first seen in the near-UV. This asymmetric behavior in the planet light curve has been explained by the presence of asymmetries in the planetary exosphere.

Motivated by this difference in transit durations, we proposed a model where the interaction of the stellar coronal plasma with the planet is able to modify the structure of the outer atmosphere of WASP-12b (Vidotto et al. 2010a; Paper1) WASP-12b is a giant planet with  $M_p = 1.41 \ M_J$  and  $R_p = 1.79 \ R_J$ , where  $M_J$  and  $R_J$  are the mass and

radius of Jupiter, respectively. It orbits its host star (a late-F star, with  $M_* = 1.35 M_{\odot}$ ,  $R_* = 1.57 R_{\odot}$ ) at an orbital radius of  $R_{\rm orb} = 0.023 \text{ AU} = 3.15 R_*$ , with an orbital period of  $P_{\rm orb} = 1.09$  d. Due to such a close proximity to the star, the flux of coronal particles impacting on the planet comes mainly from the azimuthal direction, as the planet moves at a relatively high Keplerian orbital velocity of  $u_K = (GM_*/R_{\rm orb})^{1/2} \sim 230 \text{ km s}^{-1}$ around the star. Therefore, stellar coronal material is compressed ahead of the planetary orbital motion, possibly forming a bow shock ahead of the planet. The condition for the formation of a bow shock is that the relative motion between the planet and the stellar corona is supersonic. Although we know the orbital radius of WASP-12b, we do not know if at this radius the stellar magnetic field is still capable of confining its hot coronal gas, or if this plasma escapes in a wind (see Paper 1). In the first case, where the coronal medium around the planet can be considered in hydrostatic equilibrium, the velocity of the particles that the planet 'sees' is supersonic if  $\Delta u = |u_K - u_{\varphi}| > c_s$ , where  $u_{\varphi} = 2\pi R_{\rm orb}/P_*$  is the azimuthal velocity of the stellar corona,  $c_s$  is the sound speed, and  $P_*$  is the stellar period of rotation. From observations of the sky projected stellar rotation velocity,  $P_* \gtrsim 17$  days (Fossati et al. 2010b). This implies that for a coronal temperature  $T \lesssim (4-5) \times 10^6$  K, shock is formed around WASP-12b. Although stellar flares can raise the coronal plasma temperature above these values, it is unlikely that a corona would be hotter than this.

If we take the observationally derived stand-off distance from the shock to the center of the planet ( $\sim 4.2~R_p$ , Lai et al. 2010) as approximately the extent of the planetary magnetosphere  $r_M$ , we showed that pressure balance between the coronal total pressure (i.e., ram, thermal, and magnetic pressures) and the planet total pressure requires that

$$B_c(R_{\rm orb}) \simeq B_p(r_M),$$
 (1)

where  $B_c(R_{\rm orb})$  is the magnetic field intensity of the star at  $R_{\rm orb}$  and  $B_p(r_M)$  is the magnetic field intensity of the planet at  $r_M$ . Note that we neglected the ram and thermal pressures in previous equation. Assuming that both the stellar and the planetary magnetic fields can be described as dipoles, from Eq. (1), we have

$$B_p = B_* \left(\frac{R_*/R_{\text{orb}}}{R_p/r_M}\right)^3 = B_* \left(\frac{1/3.15}{1/4.2}\right)^3 \simeq 2.4B_*,$$
 (2)

where  $B_*$  and  $B_p$  are the magnetic field intensities at the stellar and planetary surfaces, respectively. Adopting the upper limit of the stellar magnetic field of 10 G suggested by Fossati et al. (2010b), our model predicts a maximum planetary magnetic field of about 24 G. It is likely that shock formation around close-in planets is a common feature of transiting systems. In fact, in a follow-up work Vidotto et al. (2010b), we showed that about 36 out of 92 known transiting systems (as of Sept/2010) would lie above a reasonable detection threshold. For these cases, the observation of bow-shocks may be a useful tool in setting limits on planetary magnetic field strengths.

# 5. MHD simulations reveal crucial differences between solar and very-cool star magnetic structures (Benjamin Beeck, Manfred Schüssler, Ansgar Reiners)

Cool main-sequence stars of spectral types F through L have a thick convective envelope or are fully convective. In many of such stars, magnetic fields of various strengths have been detected. In the Sun, the surface magnetic field is observed to be highly

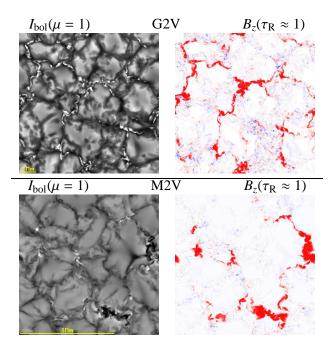


Figure 3. Snapshots of the bolometric intensity  $I_{bol}(\mu=1)$  (right panels) and vertical component  $B_z(\tau_R \approx 1)$  of the magnetic field at the optical surface (left panels) for MHD models of (G2V, upper panels) and an M2 dwarf (lower panels).

structured owing to its interaction with the convective flows. In contrast to the Sun, the structure and properties of magnetic fields on cool stars are unknown. In the absence of spatially resolved observations, the effect of the magnetic structure on signatures of the magnetic field can be evaluated by numerical simulations of the magneto-convective processes. Using the MHD code MURaM, we carried out 3D radiative magnetohydrodynamic simulations of the convective and magnetic structure in the surface layers (uppermost part of the convection zone and photosphere) of main-sequence stars of spectral types F3 to M2. The code is a "box-in-the-star" code that solves the equations of (non-ideal) MHD in three spatial dimensions with constant gravitational acceleration. It includes compressibility, partial ionization, and non-grey radiative energy transport (for details see Vögler et al 2005). To fit the surface conditions for different stellar spectral types, gravity and effective temperature were adjusted and the opacity bins were recalculated. The size of the computational box and the spatial resolution were modified in order to cover the relevant length scales of the different convection patterns.

The model grid comprises six main-sequence stars of spectral types F3, G2, K0, K5, M0, and M2. The start models were run with  $\mathbf{B} \equiv \mathbf{0}$  until a quasi-stationary state was reached. Then, a homogeneous vertical magnetic field with the field strength  $B_0 = 20 \,\mathrm{G}$ ,  $100 \,\mathrm{G}$ , or  $500 \,\mathrm{G}$  was introduced.

The modelled magneto-convection shows significant differences between M-dwarfs and stars of earlier spectral types, e. g. the Sun. As illustrated by Fig. 3, the initially homogeneous magnetic flux is accumulated into very few structures of high field strength, the cause of which are stable downflows. While solar magnetic structures appear as bright features, the magnetic structures on M-dwarfs tend to be rather dark. In the case

of the Sun, magnetic structures create a strong depression of the optical surface with hot side walls that can radiatively heat the interior of the magnetic structure. Owing to higher densities and shallower temperature gradient, this side wall heating is much less efficient for the magnetic structures in M-dwarf atmospheres. Since the magnetic field suppresses convective energy transport, the structures cool down.

These findings indicate that plage regions on M-stars might not show bright points but rather "pores" and small "star spots" of reduced intensity, which has a crucial impact on the interpretation of observational data such as M-dwarf spectra.

#### 6. Generalized 3-D Radiative Transfer for Astrophysical Atmospheres (E. Baron)

PHOENIX is a generalized model atmosphere code which works in 1 or 3 spatial dimensions. The philosophy behind PHOENIX is that it should work in a wide range of astrophysical environments and that it should handle both static and moving flows in full relativity. PHOENIX is well calibrated on many astrophysical objects: Planets/BDs, Cool Stars, Hot Stars ( $\beta$ CMa,  $\epsilon$ CMa),  $\alpha$ -Lyrae, Novae, and SNe (Iabc, IIP, IIb) (see Hauschildt & Baron 2010 an references therein). Much of the development work on PHOENIX has been devoted to handling radiative transfer in velocity flows. Velocities are important in many astrophysical objects: novae, supernovae, AGN, and  $\gamma$ -ray bursts. But of course velocities are also important in stars since the linewidth is determined by the convective velocity field as shown by Stein & Nordlund (2000).

There are two ways to deal with velocity fields: the Eulerian formulation and the co-moving formulation. Each has advantages and disadvantages. In the Eulerian formulation wavelengths are uncoupled, significantly reducing memory requirements: however, opacities are angle dependent, significantly increasing computational requirements. It is also extremely difficult to handle relativity in the Eulerian formulation. In the co-moving formulation one can include both special and general relativity exactly and opacities are isotropic, significantly reducing computational requirements; however, wavelengths are coupled, significantly increasing memory requirements. While the solution of the radiative transfer equation in the co-moving frame in 1-D has been understood for quite some time (Mihalas 1980); in 3-D it is much more complex and has been mostly approached via the cumbersome tetrad formalism (Morita & Kaneko 1984, 1986). A much simpler approach via affine parameters was developed in (Chen et al. 2007) and implemented in (Baron et al. 2009). The Eulerian Formulation is valid for velocities  $v < 1000 \text{ km s}^{-1}$  and thus is of interest in stars with low velocities. The Eulerian formulation trades off the high memory requirement of the co-moving frame for the explicit coupling of angles and frequencies, that is, all momentum space variables are coupled. Thus, at each spatial point opacities must be calculated for each coupled wavelength direction point, leading to both a large amount of computation and storage. Nevertheless PHOENIX has been adapted to include the Eulerian formulation in 3-D (Seelmann et al. 2010).

In summary, PHOENIX 3-D solves the generalized atmosphere problem with both co-moving and Eulerian formulations in Cartesian, spherical, and cylindrical geometry. We still need to study which approach is computationally better, which may depend on the particular computer architecture, particularly with the advent of GPUs and very low memory per core exoscale computing. The next step is to go beyond test problems to production code. While full 3-D RT is too computationally complex for radiation hydrodynamics, some of the methods we have developed may be adapted to a more

simplified approach. It is crucial to do full radiative transfer to determine abundances, perform detailed hydrodynamic model verification, and for other applications to observed data.

#### 7. Multi-D hydro-simulations of substellar atmospheres (Adam P.Showman)

Over 100 transiting hot Jupiters are now known, and observations from the Spitzer and Hubble Space Telescopes and groundbased facilities constrain the atmospheric composition and three-dimensional temperature structure of many such objects. Phase curves show that some hot Jupiters, such as HD 189733b, have modest (~200 K) day-night temperature variations (e.g., Knutson et al. 2007), while others have much larger day-night temperature differences. For the case of HD 189733b –the best-observed hot Jupiter– the Spitzer infrared light curves imply that the hottest region is not at the substellar point but rather is displaced 30 degrees of longitude to the east. This feature provides strong evidence of atmospheric circulation on these tidally locked planets.

The atmospheric dynamical regime of hot Jupiters differs from that of, for example, brown dwarfs. The atmospheric circulation on hot Jupiters is probably driven primarily by the  $\sim 10^5-10^6$  W/m² net radiative heating on the dayside and cooling on the nightside; unlike the case of Jupiter or typical brown dwarfs, the absorbed stellar flux exceeds the convective fluxes in the planet's interior by 3-5 orders of magnitude. Evolution and structure models indicate that multi-Byr-old hot Jupiters have deep radiative zones extending from the top of the atmosphere to pressures of typically 100-1000 bars. Thus, the weather near the infrared photosphere on hot Jupiters occurs in a stably stratified radiative zone. Hot Jupiters are thought to be synchronously rotating with their 1-10-day orbital periods, implying that planetary rotation is less dominant in their dynamics than is the case for Jupiter or typical brown dwarfs.

A variety of 3D dynamical models of the atmospheric circulation on hot Jupiters have been published (e.g., Showman and Guillot 2002; Dobbs-Dixon & Lin 2008; Showman et al. 2008, 2009; Rauscher & Menou 2010; Thrastarson and Cho 2010). These models typically model the circulation of hot Jupiters on 2-4-day orbits assuming the interior is tidally locked. At the pressure of the infrared photosphere, the circulation in these models typically exhibits a banded structure, with 1-3 broad east-west jet streams whose speeds reach several km/sec. Day-night temperature differences are commonly hundreds of K at the photosphere. Real hot Jupiters probably exhibit a wide diversity of behaviors, which have yet to be thoroughly explored in circulation models.

Interestingly, the eastward offset of the hot region from the substellar longitude inferred from infrared light curves of HD 189733b – which provides our current best evidence for atmospheric circulation on hot Jupiters – was predicted five years before its discovery (Showman and Guillot 2002). In their model, the eastward offset results from advection by a robust, eastward flowing equatorial jet stream that dominates the circulation (Fig. 4). Subsequent models by several groups have generally confirmed the robustness of this feature (e.g., Showman et al. 2008, 2009; Dobbs-Dixon and Lin 2008; Rauscher and Menou 2010). However, to date, the mechanism for this so-called "equatorial superrotation" has not been identified. New, unpublished work by A.P. Showman and L.M. Polvani shows, however, that the superrotation results from standing Rossby waves generated by the day-night thermal forcing. The Rossby waves, which are planetary in scale, generate phase tilts such that equatorward-moving air exhibits greater eddy angular momentum than poleward-moving air. This pumps eddy

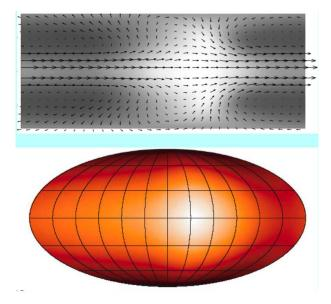


Figure 4. (Bottom): Longitudinal temperature structure of of hot Jupiter HD 189733b inferred from Spitzer 8-micron infrared light curve (Knutson et al. 2007), showing eastward offset of hottest region from substellar longitude. (Top) Temperature pattern (greyscale) and winds (arrows) from three-dimensional circulation model of a hot Jupiter by Showman and Guillot (2002). A common feature of such models is the eastward equatorial jet, which displaces the hottest regions to the east of the substellar point, as seen in the observations.

angular momentum from the midlatitudes to the equator and generates the equatorial superrotating jet. Showman and Polvani demonstrated the mechanism in an idealized, linear, analytic model, in simplified nonlinear models, and in full three-dimensional general circulation models. An implication is that the mechanism for producing the jet need not involve turbulent cascades or other eddy-eddy interactions, but rather results from a direct interaction between the standing, thermally generated quasi-linear eddies and the mean flow at the planetary scale.

#### 8. Weather on a Hot Jupiter (Eric Agol)

Testing global models of weather on hot jupiters requires observations of their global properties. To date, the best means available for such a comparison is infrared observations of the phase variation of hot jupiters (Knutson et al. 2007). If the weather pattern changes on a timescale slower than the orbital time of the planet, then during the orbit the different faces of the planet will be observed, allowing a deconvolution of the longitudinal brightness of the planet (Cowan & Agol 2008). Since the planet cannot be resolved from the star, there are several possible ways such an analysis might go wrong: (1) stellar variability might swamp the planet phase variation; (2) planet variability might invalidate the steady-state assumption required for inversion; (3) planet-star interaction might cause stellar brightness variations on a similar timescale as the planet's orbit. In addition, instrumental effects can be present which may be stronger than the phase variation. So far the best target for this sort of observation is the exoplanet HD

189733b. It orbits a bright star, it is large in size compared to its host star, and it is hot enough and has a short enough period to enable observations of a reasonable duration. However, the host star is strongly variable in the optical,  $\sim 1-2\%$ , with a period of about 12 days, so the host star variability must be accounted for to properly measure the planet's infrared variability with the Spitzer Space Telescope. We measured the phase variation over slightly longer than half an orbital period at 8  $\mu$ m with IRAC Channel 4 (Knutson et al. 2007), and then observed a subsequent six transits and six eclipses with the goals of determining the day-side variability and looking for transit-timing variations (Agol et al. 2008, Agol et al. 2010). We also obtained simultaneous ground-based monitoring in the optical which we used to correct for the stellar variability by extrapolating the optical stellar variation into the infrared (Winn & Henry 2008).

Based on these data, we found that the absolute flux of the system could be measured to <0.35 mmag after decorrelating with instrumental variations and stellar variability. We used this decorrelation to correct for the stellar variability, giving a more precise phase variation (Figure 5). The observed phase function is in good qualitative agreement with models of weather on this hot jupiter (e.g. Showman et al. 2009), albeit with an observed peak of the planet's flux that is closer to the secondary eclipse than predicted by the models. The location of this peak is primarily controlled by the ratio of the radiative timescale to the advection timescale,  $\epsilon$ , so the data indicate that the models either overpredict the super-rotation speed of the equatorial jet, or they overpredict the cooling timescale at the 8 micron photosphere. We also find an offset in the secondary eclipse time; after correcting for light-travel time across the system, the offset can be accounted for by the asymmetric dayside flux caused by the super-rotating jet (this offset is due to the fact that we fit the secondary eclipse with a model in which the planet is uniform in surface brightness). The night side is about 64% of the brightness of the day side and the secondary eclipse depth variation has an RMS of < 2.7%, which is limited by the photometric precision of the data. These results are in good agreement with general circulation models for this planet which predict fluctuations of <1%.

## 9. Overshoot, gravity waves and non-equilibrium chemistry (Derek Homeier, France Allard, Bernd Freytag)

The PHOENIX BT-Settl models (Allard et al. 2010) combine a cloud formation and gas phase non-equilibrium chemistry model, using vertical diffusion profiles based on CO5BOLD RHD simulations as an input to our models, finding the mixing in the transition zone from carbon monoxide- to methane-dominated chemistry to be governed by gravity waves forming in the upper atmosphere (Freytag et al. 2010). We introduce updated reaction rates for the CO to  $CH_4$  conversion from Visscher et al. (2010) and include departures from chemical equilibrium in the CO to  $CO_2$  ratio to determine the molecular fractions of  $CH_4$ , CO and  $CO_2$  for atmospheres spanning the range from L to T dwarfs. Synthetic spectra calculated for the resulting compositions reproduce the observed upmixing of carbon monoxide in brown dwarfs across the L/T transition. In addition we find carbon dioxide to appear in excess of its CE abundance in T dwarfs. The models produce an improved fit to the observed mid-infrared photometry of the coolest brown dwarfs (Burningham et al. 2010), and are confirmed by the identification of distinctive  $4.2 \,\mu m$   $CO_2$  absorption features in several late T dwarf spectra by the AKARI satellite (Yamamura et al. 2010).

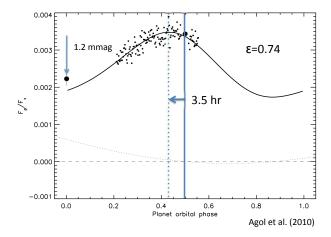


Figure 5. Measured phase-variation of HD 189733b (dots) at 8  $\mu$ m after correction for stellar variability (dotted line). The peak of the phase function is offset 3.5 hours before secondary eclipse (orbital period: 53 hours). The night-side is 1.2 mmag fainter than the dayside, or about 64% of the flux. The phase variation may be fit by a toy model (solid line; Cowan & Agol 2010) in which the energy is advected in a super-rotating jet in which the ratio of the radiative to advection times  $\epsilon = 0.74$ .

Acknowledgments. EB was supported by NSF grant AST-0707704, US DOE Grant DE-FG02-07ER41517, and by program number HST-GO-12298.05-A which is supported by NASA through a grant from the Space Telescope Science Institute, which is operated by the Association of Universities for Research in Astronomy, Incorporated, under NASA contract NAS5-26555. This research used resources of the NERSC, which is supported by the Office of Science of the U.S. Department of Energy under Contract No. DE-AC02-05CH11231; and the Höchstleistungs Rechenzentrum Nord (HLRN). Support for EA was provided by NSF through CAREER Grant No. 0645416 and by NASA through an award issued by JPL/Caltech. APS acknowledges funding from NASA Origins. D. H. gratefully acknowledges support from a foreign travel grant by the DAAD. F. A. and B. F. acknowledge financial support from the ANR, and the PNPS of CNRS/INSU, France. Stellar and substellar atmosphere models for this study have been calculated at the GWDG.

#### References

Agol, E., Cowan, N. B., Bushong et al. 2009, vol. 253 of IAU Symposium, 209

Agol, E., Cowan, N. B., Knutson, H. A. et al. D. 2010, ApJ, 721, 1861

Allard, F., Homeier, D., & Freytag, B. 2010 this vol. 1011. 5405

Baron, E., Hauschildt, P. H., & Chen, B. 2009, A&A, 498, 987

Berdyugina S. V., Berdyugin A. V., Fluri D. M., Piirola V. 2011, ApJ submitted

Berdyugina S. V., in Polarimetry of cool atmospheres: From the Sun to exoplanets, eds. J.R. Kuhn, 2011, (arXiv:1011.0751)

Berdyugina, S. V., Berdyugin, A. V., Fluri, D. M., Piirola, V. 2008, APJ 673, L83

Berdyugina, S. V. 2005, Liv. Rev. Solar Phys. 2, 8

Berger, J. P., Haguenauer, P., Kern, P. et al. 2001, A&A, 376, L31

Burningham, B., Leggett, S. K., Homeier et al. 2010, submitted to MNRAS.

Chelli, A., Duvert, G., Malbet, F., & Kern, P. 2009, A&A, 498, 321

Chen, B., Kantowski, R., Baron, E., Knop, S., & Hauschildt, P. 2007, MNRAS, 380, 104

Cowan, N. B., & Agol, E. 2008, ApJ, 678, L129

— 2010, arXiv:1011.0428

Dobbs-Dixon, I. & Lin, D.N.C. 2008. ApJ 673, 513.

Fossati, L., Haswell, C. A., Froning, C. S., & et al. 2010, ApJ, 714, L222

Fossati, L., Bagnulo, S., Elmasli, A., & et al. 2010, ApJ, 720, 872

Freytag, B., Allard, F., Ludwig, H., Homeier, D., & Steffen, M. 2010, A&A, 513

Hauschildt, P. H., & Baron, E. 2010, A&A, 509, A36

Hebb, L., Collier-Cameron, A., Loeillet, B., & et al. 2009, ApJ, 693, 1920

Henry, G. W., & Winn, J. N. 2008, AJ, 135, 68

Homeier, D., Freytag, B., & Allard, F. 2010 this vol. suppl.

Kloppenborg, B., Stencel, R., Monnier, J. D. et al. 2010, Nat, 464, 870

Knutson, H. A., Charbonneau, D., Allen, L. E. et al. 2007, Nat, 447, 183

Kraus, S., Hofmann, K., Menten, K. M. et al. 2010, Nat, 466, 339

Kuhn, J. R., Geiss, B., Harrington, D. M. 2011, in Solar Polarization 6, eds. Kuhn et al., (arXiv:1010.0705)

Kuhn, J. R., Berdyugina, S. V., Fluri, D. M., Harrington, D. M., Stenflo, J. O. 2007, ApJL 668, L63

Lai, D., Helling, Ch., & van den Heuvel, E. P. J. 2010, ApJ, 721, 923

Mihalas, D. 1980, ApJ, 237, 574

Monnier, J. D., Berger, J. P., Millan-Gabet, R. 2003, in Proc. SPIE, Interferometry for Optical Astronomy, W.A. Traub, editor, Vol. 4838, 1127–1138

Monnier, J. D., Zhao, M., Pedretti, E. et al. 2007, Science, 317, 342

Morita, K., & Kaneko, N. 1984, Ap&SS, 107, 333

— 1986, Ap&SS, 121, 105

Pedretti, E., Monnier, J. D., Brummelaar, T. T., & Thureau, N. D. 2009, Nat, 53, 353

Pedretti, E., Monnier, J. D., Lacour, S. et al. 2009, MNRAS, 397, 325

Rauscher, E. & Menou, K. 2010, ApJ 714, 1334

Seelmann, A., Hauschildt, P. H., & Baron, E. 2010, A&A, 522, A102

Scholz, R., McCaughrean, M. J., Lodieu, N., & Kuhlbrodt, B. 2003, A&A, 398, L29

Showman, A. P., Fortney, J. J., Lian, Y. et al. 2009, ApJ, 699, 564

Showman, A.P. et al. 2008, ApJ 682, 559

Showman, A.P., & Guillot T. 2002, A&A 385, 166.

Stein, R. F., & Nordlund, Å. 2000, Sol. Phys., 192, 91

Thrastarson, H.T. & Cho, J.Y-K. 2010 ApJ, 716, 144

Vidotto, A. A., Jardine, M., & Helling, Ch. 2010, ApJ, 722, L168 (Paper 1)

— 2010, MNRAS Letter, in press. arXiv:1011.3455

Visscher, C., Moses, J. I., & Saslow, S. A. 2010, Icarus, 209, 602. 1003.6077

Vögler, A., Shelyag, S., Schüssler, M. et al. 2005, A&A, 429, 335

Wiktorowicz, S. J. 2009, ApJ 696, 1116

Woitke, P. & Helling, Ch 2004, A&A 414, 335

Yamamura, I., Tsuji, T., & Tanabé, T. 2010, ApJ, 722, 682, 1008, 3732

Zhao, M. 2009, PhD thesis, University of Michigan